13

Motion Planning of Intelligent Explorer for Asteroid Exploration Mission

Takashi Kubota, Tatsuaki Hashimoto and Jun'ichiro Kawaguchi
Japan Aerospace Exploration Agency
Japan

1. Introduction

In-situ observations of minor bodies like asteroids or comets are scientifically very important because their sizes are too small to have high internal pressures and temperatures, which means they should hold the early chemistry of the solar system. In recent years, some rendezvous or sample-return missions to small body have received a lot of attention in the world. To date, the missions of NEAR (Farquhar, 2001), Deep Space 1 (Rayman et al., 2000), Deep Impact (Chiu et al., 2000), and Stardust (Atkins, et al., 2000) have been successfully performed, while MUSES-C (Kawaguchi et al., 2000) and Rosetta (Wittmann, et al. 1999) are currently in operation. NEAR spacecraft was successfully put into the orbit of the asteroid 433 Eros in February 2000. After precise remote-sensing observations, NEAR spacecraft succeeded in hard-landing on the surface of EROS in February 2001. In Japan, meanwhile, ISAS (Institute of Space and Astronautical Science) launched an asteroid sample and return spacecraft MUSES-C toward a near Earth asteroid 1998SF36 in 2003 and performed soft landing on the asteroid in 2005.

In deep space missions, ground based operation is very limited due to the communication delay and low bit-rate communication. Therefore, autonomy is required for deep space exploration. On the other hand, because little information on the target asteroid is known in advance, robotics technology is used for the spacecraft to approach, rendezvous with, and land on the asteroid safely. Various kinds of advanced and intelligent robotics technologies (Kubota et al. 2001) have been developed and used for navigation and guidance of the explorer to touch down and collect samples. This chapter describes the outline of the sample return mission MUSES-C, descent and touch-down scenario, vision based navigation scheme, sensor based motion planning, autonomous functions, and flight results in detail.

This chapter is structured as follows. Section 2 describes the mission purpose and the configuration of MUSES-C spacecraft. In Section 3, navigation sensors are explained. In Section 4 discusses the strategy for autonomous approach and landing. Autonomous descent scheme based on navigation sensors is introduced. In Section 5, a vision based navigation scheme is presented. In Section 6, flight results in MUSES-C mission is presented. Finally, Section 7 is for discussions and conclusions.

2. MUSES-C Mission

2.1 Outline of MUSES-C Mission

ISAS launched the MUSES-C spacecraft toward the asteroid in May 2003, which is named "Hayabusa". The MUSES-C project (Kawaguchi et al., 1998) is aiming at demonstrating four key technologies required for the future sample and return missions from extra-terrestrial bodies. Those technologies are : 1) solar electrical propulsion with ion thrusters in an interplanetary space, as a primary propulsive means, 2) autonomous optical guidance and navigation, 3) automated sampling mechanism, and 4) direct hyperbolic reentry of the recovery capsule to the ground.

The target body of the MUSES-C spacecraft is a near Earth asteroid 1998SF36 which is named "Itokawa". The launch date was May 9th in 2003 and the arrival at 1998SF36 in September 2005. Leaving the asteroid in December 2005, the spacecraft returns to the Earth in June 2010. The mission duration from launch to the Earth return is about 7 years. In MUSES-C mission, the spacecraft Hayabusa has stayed for about four months around the asteroid and both mapping and sampling operations were carried out during that short period. Figure 1 shows the illustration of MUSES-C mission.

Hayabusa was launched via the ISAS medium class launch vehicle M-V. The mass of the spacecraft is about 500[kg] including chemical and ion engine propellant of 130[kg]. The solar cell is a tri-junction one and the solar panel generates approximately 1.8[kW]. During the flight, the distance from the earth is shorter than 2[AU].

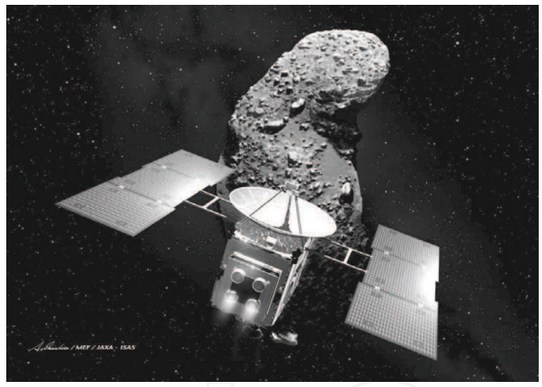

Figure 1. MUSES-C Mission (Ikeshita/MEF/JAXA)

2.2 MUSES-C Spacecraft

In deep space, it is difficult to operate a spacecraft on a real-time basis remotely from the earth mainly due to the communication delay. So autonomous navigation and guidance are required for descent and touch-down to the asteroid. For this purpose, MUSES-C has some navigation sensors and onboard image processing system (Hashimoto et al., 2000). The rendezvous and touch down to the asteroid, whose size, shape, surface condition are unknown, requires intelligent and advanced navigation, guidance and control system. Figure 2 shows the overview and the configuration of the MUSES-C spacecraft.

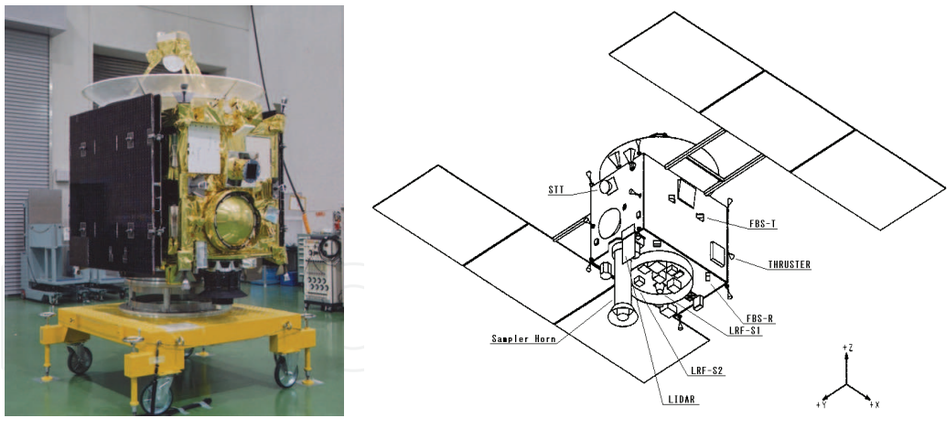

Figure 2. Overview and Configuration of MUSES-C Spacecraft

2.3 AOCS and GNC System

When the spacecraft was designed, the exact size, the shape, and the surface condition of the target asteroid were unknown. The GNC system was designed so that it could cope with various situations within the severe weight and power restrictions for the spacecraft. Figure 3 shows the AOCS and GNC system of Hayabusa spacecraft. TSAS (Two axis Sun Aspect Sensor), STT (Star Tracker) and IRU (Inertial Reference Unit) are combined to determine the spacecraft attitude. ACM (AcceleroMeter) is used to accurately measure the velocity increment gained by RCS (Reaction Control System) firings. RW (Reaction Wheel) and RCS thrusters are used for attitude and position control. Twelve thrusters were installed on the spacecraft and this arrangement allows the control of translational and rotational motion independently.

Some navigation sensors (Hashimoto et al., 2003) for descent and touchdown are equipped on Hayabusa spacecraft. The spacecraft has two kinds of optical navigation cameras. The narrow angle camera (ONC-T) is used for mapping (Maruya et al., 2006) and multiple scientific observations of the asteroid from the Home Position. The wide angle cameras (ONC-W1 and ONC-W2) are both used for onboard navigation, though W2 is used only when high-phase angle observation. Control electronics for ONCs (ONC-E) equipped with a RISC processor and a Gate Array image processor has some image processing functions such as image compression, center-finding of bright object, correlation tracking, feature terrain extraction, etc. Measurement of the altitude is performed with LIDAR (Light radio Detecting And Ranging). LIDAR covers the measurement range from 50[m] to 50[km]. For sampling the surface materials, cancellation of the relative horizontal speed is essential while touch down. To accomplish this requirement, the spacecraft drops a Target Marker (TM) that can act as a navigation aid by posing as an artificial landmark on the surface. The position of TM is estimated by using ONC. Since it is not so easy to detect TM from several tens of meters altitude, TM is equipped with reflexive reflector and ONC has a flash lamp (FLA) whose radiation is synchronized with camera exposure. Laser Range Finder (LRF) is used at lower altitude. LRF has four beams that are canted with 30 [deg] and can measure the range from 7[m] to 120[m]. LRF can provide the height and attitude information with respect to the surface. Four sets of Fan Beam Sensors (FBS) are equipped onboard as alarm sensors to detect some potential obstacles that may hit the solar cell panels.

The GNC logic is implemented in AOCU (Attitude and Orbit Control Unit), where a high performance microprocessor is equipped. Figure 4 shows the block diagram of GNC functions. The core of onboard navigation system is an extended Kalman filter. The filter outputs the estimated position and velocity relative to Itokawa. The state dynamics for the Kalman filter employs orbit dynamics model around Itokawa. Simple gravity field model is included in the dynamics. The observations for spacecraft position come from ONC, LIDAR and LRF.

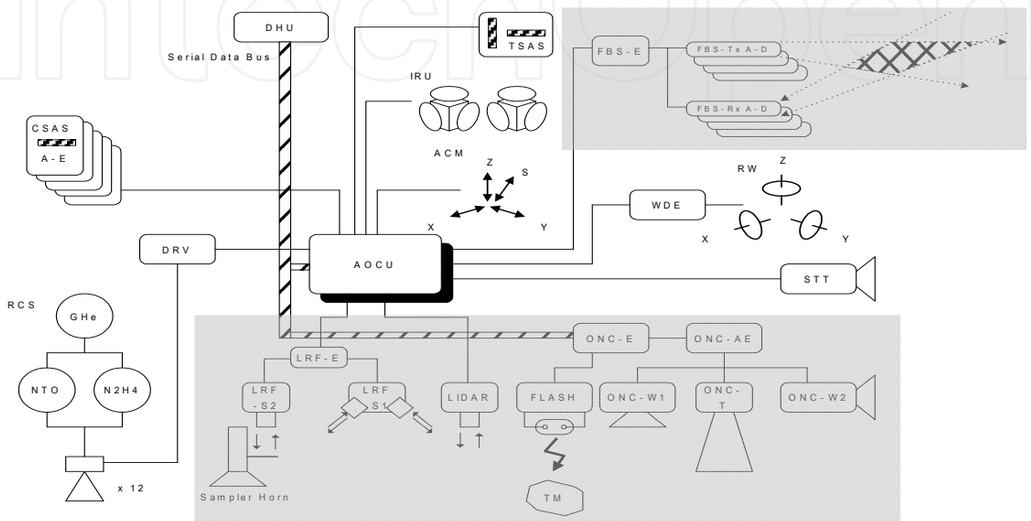

Figure 3. AOCS and GNC System of Hayabusa Spacecraft

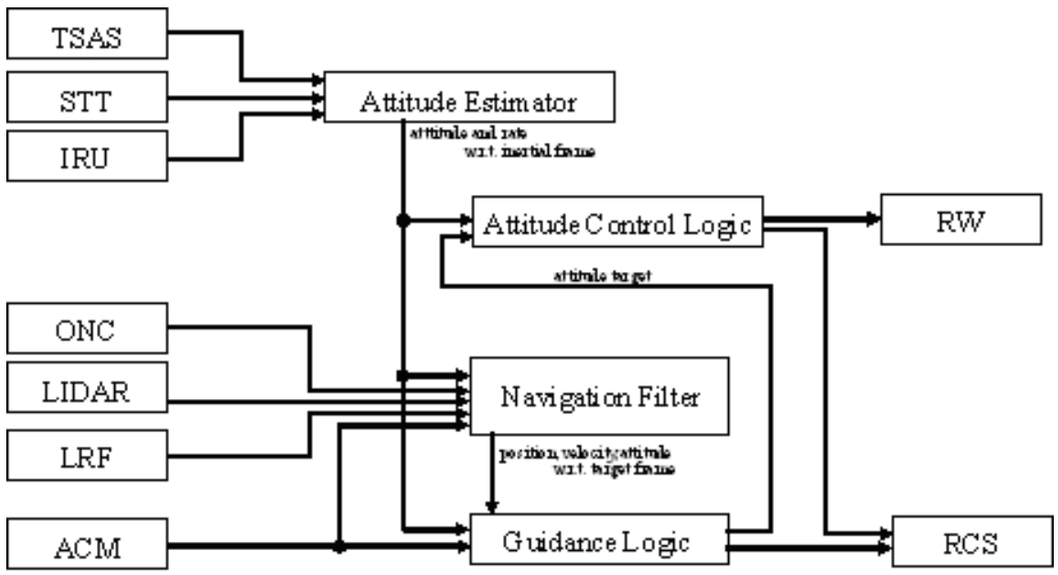

Figure 4. Block Diagram of AOCS/GNC System

3. Navigation Sensors

For autonomous descent and touchdown, various kinds of navigation sensors are used. The specifications of the main sensors for navigation are described as follows.

3.1 ONC-W

Hayabusa spacecraft has one telescopic camera ONC-T and two wide FOV cameras: ONC-W1 and W2. ONC-W1 whose FOV aligned to -Z axis of the spacecraft is used for on-board navigation. ONC-W2 has the FOV of -Y direction, which is used for terminator observation phase. The FOV of ONC-W1 is 60deg x 60deg and the resolution is 1000(H) x 1024(V). The overview of ONC-W1 is shown in Figure 5.

3.2 LIDAR

LIDAR is a pulse laser radar which measures the traveling time of the pulse between the spacecraft and the asteroid surface. A Photo of the prototype model is shown in Figure 5. Since the magnitude of received signal will change about 10^6 orders between 50km and 50m, LIDAR has automatic gain control function of APD. Transmitting pulse can be synchronized with external signal such as AOCS timing. This function is not only for precise range measurement but also synchronization with the exposure of ONC-T or NIRS, which helps the alignment measurement of both sensors. To minimize the weigh of optics, the reflecting mirror is made of SiC.

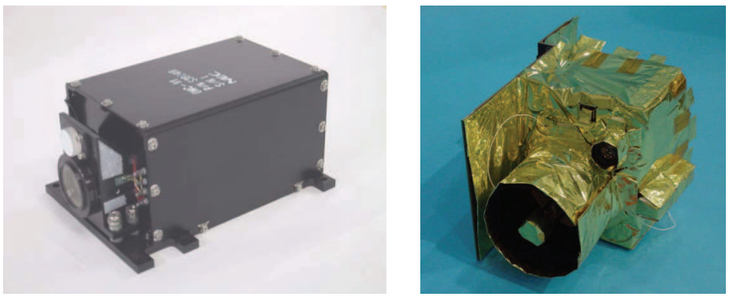

Figure 5. Overviews of ONC-W (Left) and LIDAR (Right)

3.3 LRF

LRF(Laser Range Finder) consists of four beams sensors for navigation(LRF-S1), one beam sensor for touchdown detection(LRF-S2), and an electronics circuit (LRF-E). Photos of LRF-S1 and LRF-S2 are shown in Fig.6. LRF detects the range to the surface with the phase deference between AM-modulated transmitting and receiving laser light. LRF-S1 has four beams canted 30deg from vertical direction and AOCU can calculate relative attitude and position to the surface using four beam range information. The target of LRF-S2 is the side surface of the sampler horn and it detects the change of the length of the horn which means that the horn is collide with the surface. LRF has single electronics and S1 and S2 are switched by commands when used.

3.4 FBS

FBS (Fan Beam Sensors) are sensors for detecting obstacles bigger than 10cm. A pair of a transmitter (FBS-T) and a receiver (FBS-R) forms a three-dimensional detection area shown in Fig.7. Four pairs of FBS cover almost half of the area beneath the spacecraft's solar cell panels as shown in Fig.8.

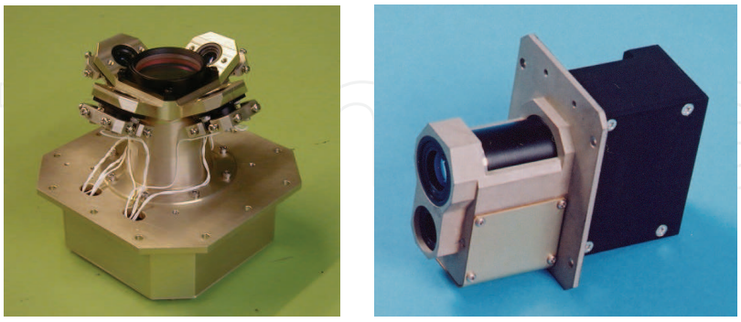

Figure 6. Overviews of LRF-S1 and LRF-S2

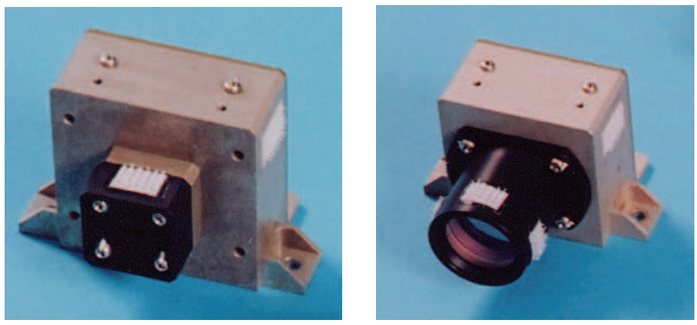

Figure 7. Overviews of FBS-T and FBS-R

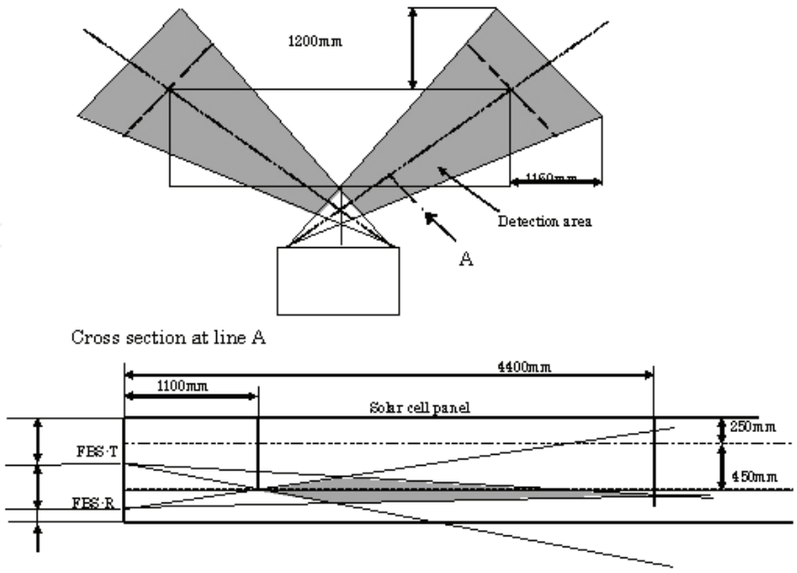

Figure 8. Detection Area of FBS

4. Autonomous Landing

For landing on an unknown body safely, it is necessary to obtain the terrain information of a planetary surface around a landing point. It is also important to guide a spacecraft to the landing point without hitting rocks or big stones. In the touch down phase, cancellation of the horizontal speed relative to the surface of the landing site is essential. Hayabusa spacecraft uses a new method to land on the surface of an unknown body autonomously, using optical cameras and laser altimeter (Hashimoto et al., 2002). The strategy for autonomous descent and touch-down consists of the following phases. The autonomous descent and landing sequence is illustrated in Fig.9.

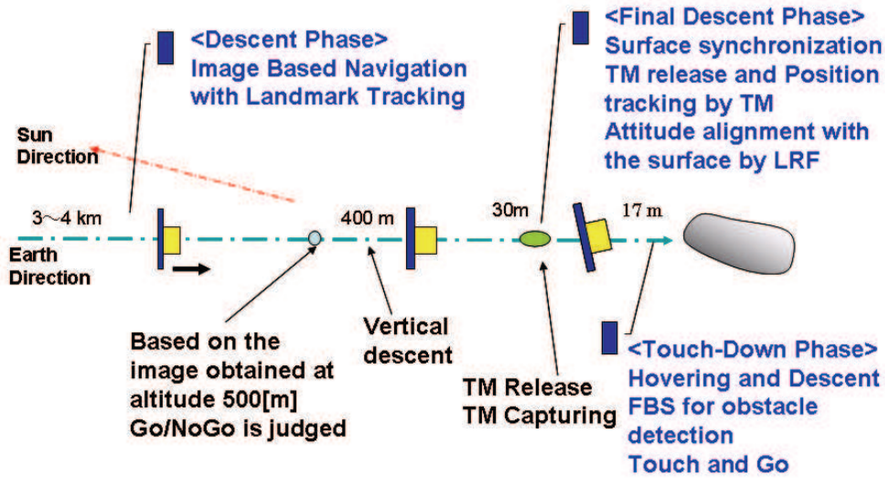

Figure 9. Scenario for final descent and touchdown

4.1 Descent Phase

While the whole of the asteroid image is in the field of view (FOV) of the optical navigation camera (ONC), the 3D navigation scheme (Hashimoto et al. 2001) based on the center-finding of the asteroid is used. After a part of the asteroid goes out of the FOV (about 1 km altitude), the spacecraft will nominally descent with only vertical velocity control because it cannot detect the direction of the asteroid center. Therefore, navigation accuracy depends upon the initial position and velocity, which are determined in the Home Position.

For an experiment, Navigation, Guidance, and Control (NGC) system has also a natural terrain tracking function. That is, characteristic features like craters on the surface are extracted from images and tracked autonomously. If some tracked features are recognized to be unsuitable for tracking, new appropriate features are extracted automatically. The line-of-sight vectors to the extracted features provide relative position to the surface. Since the locations of the features are unknown in the asteroid-fixed coordinate system, the spacecraft measures only the deviation of the vectors, that is, it can obtain relative velocity to the surface.

4.2 Final Descent Phase

The sampling method in MUSES-C mission is a so-called touch-and-go way. That means the spacecraft shoots a small bullet to the surface just after the touch-down is detected, collects ejected fragments with a sampler horn, and lifts off before one of solar cell panels hits the

surface. Therefore, the control of the vertical velocity and the cancellation of the horizontal speed are essential for both successful sampling and the spacecraft safety. To meet these requirements, TM is released from the spacecraft at the altitude of about 30[m]. At the altitude of about 30[m], ONC tries to capture TM, that would be placed near the target landing point. To ensure the visibility of TM, the surface of TM is covered with reflexive reflector and ONC provides the differential image taken by flash-on and flash-off.
After TM is successfully captured, the relative navigation logic is initiated to obtain the position with respect to TM and the local horizon, which is calculated based on the asteroid model. The spacecraft moves to the position right above the TM, and then the attitude of the spacecraft is aligned to the local horizon determined from Laser Range Finder (LRF) measurements. The spacecraft is guided to the landing point and stays there until the relative velocity is stabilized within a limit. The introduction of an artificial landmark drastically reduces the computational load and uncertainty of image processing, even though the function of natural terrain tracking (Misu et al., 1999) remains as an experiment and backup.

4.3 Touchdown Phase

After the alignment, the spacecraft starts descending again and touches down the asteroid surface to collect samples. During the touchdown descent, some potential obstacles are checked with Fan Beam Sensors (FBS). If any obstacle is detected, the touchdown and sampling sequence is terminated and emergency assent is initiated. When the touchdown is detected, the spacecraft collects the sample as soon as possible and then lifts off. Figure 10 shows the sensors used for touchdown detection (Uo et al., 2006). Before the touchdown descent, AOCU changes the sensor from LRF-S1 to LRF-S2, which can sense the distance between LRF and the target on the horn and also sense the brightness of the target on the horn. LRF-S2, ACM and IRU are used for touchdown detection.

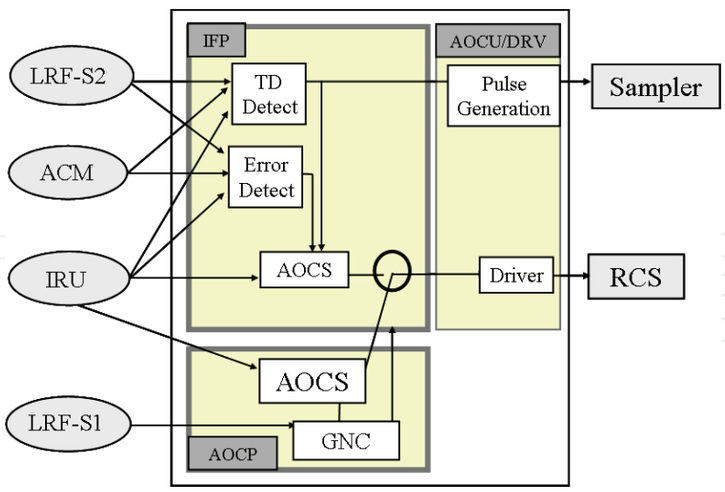

Figure 10. Touchdown Detection Scheme

4.4 Sampling Phase

A sample collection technique is what the MUSES-C spacecraft demonstrates first in the world. Different from the large planets, the asteroid is a very small object whose gravity field is too little for any sampler to dig and drill the surface. Nevertheless, the spacecraft has

to cope even with the hard surface such as rocks, while it is requested to function for soft surface like sands as well. Therefore, a novel sample collection system is introduced as shown in Fig.11. The introduced method is the combination of the Shooting Projectile and the Fragment Catcher. The basic idea is retrieving fragments from the surface ejected by the projectile shot. And a key in the mechanism is the use of the catcher whose inlet surface covers the shot area that is concealed from the main body of the spacecraft, so that the fragments and dusts cannot hit the spacecraft at all. The spacecraft extends a mast whose tip end is equipped with a gun shooting a projectile of 10[g] at the speed of 300[m/sec]. A tiny hole that opens above a flange relieves the high-pressured gas after the shot. It has deceleration device inside that absorbs the fragments/projectile kinetic energy.

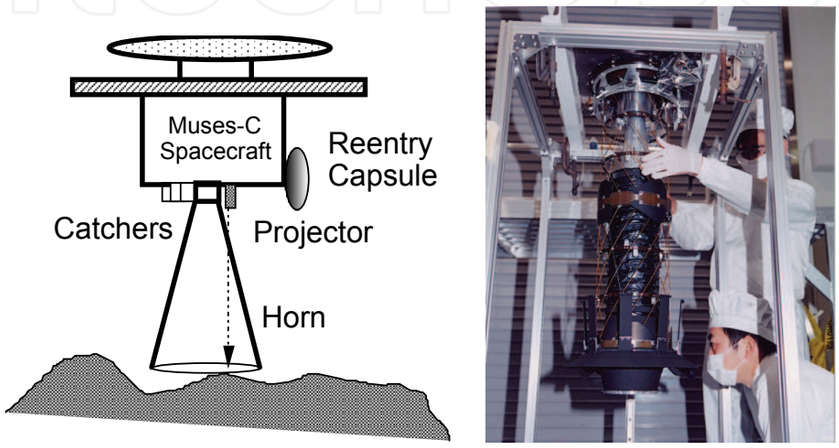

Figure 11. Sample Collection System

4.5 Descent and Touchdown Sequence

Figure 12 shows the operation sequence below the height of 500[m]. First, onboard navigation system is initialized by ground command. Initial position and velocity is calculated using GCP navigation. The onboard guidance logic is then initiated, and the descending begins. The GNC system keeps the constant descending velocity. In this case, the descending velocity is set at 0.1[m/s]. When the spacecraft reaches the height of 100[m], the spacecraft checks if the "continue" command is sent from the ground. If the continue command is not received by this time, the spacecraft interrupts descending and return to Home Position. At a height of 40[m], the wire that ties target marker on the spacecraft is cut. Right after that, the spacecraft decreases the descending velocity. Thus the target marker leaves the spacecraft and continues to fall on to the surface at a speed of about 10[cm/s]. The spacecraft begins slow free fall. During the free fall, the spacecraft examines if the LRF data is valid, and the consistency between the LRF data and the navigation solution generated using LIDAR data. If the consistency is within an expected range, the navigation filter begins to use LRF data instead of LIDAR data. Using the LRF based navigation solutions, the spacecraft hovers at a height of 17[m]. In this hovering point, the spacecraft waits the target marker to reach the surface. ONC is changed to the TMT mode after the TM separation. When the target marker image is acquired by ONC, after the interval to wait for the TM to reach the surface, relative position with respect to the target marker is determined combined with the LRF data. The Six DOF controller is activated after the navigation filter solution converges.

Several abort functions are implemented on the spacecraft. The spacecraft stops the sequence and returns to home position in the following events. These functions are automatically enabled and disabled according to the progress of the sequence.

1. Loss of LIDAR observation
2. Loss of LRF observation
3. Loss of ONC observation
4. Obstacle detection by FBS
5. Large error of attitude and attitude rate

Nominal Altitude	Nominal Velocity	Activity
500	0.05 0.1	Initialize navigation filter by ground command Initiate onboard guidance logic and start vertical descent
70	0.1	Check if "continue" command is set from the ground
40	0.1	Cut wire that ties Target Marker to the spacecraft
	0.06	Decrease spacecraft velocity from 0.1 m/s->0.06m/s (TM continues to descend at 0.1 m/s)
35	0.06	Check if LRF data is consistent with current navigation solution
30	0.06	Initialize navigation filter for altitude keeping
17	0	Keep hovering altitude and wait TM reach the surface
17	0	Start TM image acquisition with ONC
17	0	Initialize final descent navigation filter Wait nav filter converges
17	0	Calculate attitude relative to local surface with LRF data
17	0	Start attitude alignment maneuver
17	0	Change LRF from navigation mode to TD mode
17	0.04	Execute descent dV of 0.04m/s for touchdown
0	< 0.1m/s	On touchdown detection, execute sampling sequence: projecter ignition escape dV

Figure 12. Operation Sequence

5. Vision based Navigation

The following image processing techniques are used for visual navigation in MUSES-C mission as shown in Fig.13.

5.1 WCT (Whole image Center Tracking)

In this mode, groups of adjoining pixels whose brightness beyond the specified threshold are extracted and the center address and the total number of the pixels of each group are calculated. Though less than nine groups are extracted as the specification, only one group, which has maximum number of pixels is usually used for center finding of the asteroid. When the image of the asteroid is divided into some portions with the illumination condition, Attitude and orbit control unit (AOCU) uses some relatively large groups and estimates real center of the asteroid.

5.2 TMT (Target Marker Tracking)

The function of this mode is basically the same as WCT mode except that TMT uses a differential image between flush-on and off. Different from the center finding of the whole asteroid image, the size of the extracted groups are expected to be a few pixels considering the distortion of the optics and the number of extracted groups must be one in order to track TM properly.

Artificial target marker is dropped down onto the asteroid surface to cancel the relative velocity. To use such a target marker, it is needed to develop a marker object with low restitution coefficient under the micro-gravity environment. To develop an object with low restitution coefficient, Japanese traditional "otedama" concept is introduced. "Otedama" is made of some amount of small beads inside a soft cover cloth. When "otedama" collides with other object, beads are expected to reduce the total collision energy as shown in Fig.14. To investigate the collision mechanism of "otedama", the dropping tower micro-G experiments were performed at MGLAB in Gifu in Japan. Experimental results show that the restitution coefficient values of "otedamas" mark below 0.1 (Kubota et al., 2007).

5.3 FWT (Fixed Window correlation Tracking)

This mode is prepared for an experiment and a backup when TM is not captured. Some tracking windows are designated on an image and the windows are used for templates of the tracking. Each window on the next coming image is correlated with corresponding template and the deviation of horizontal and vertical pixels between images are calculated. FWC is used to measure the relative velocity against the surface.

5.4 AWC (Auto Window Tracking)

Auto window tracking (AWC) (Misu et al., 1999) is also prepared for an experiment and a backup and the function of the correlation tracking is the same as FWC. AWC autonomously sets tracking windows. Firstly, some edges are extracted on the image, and the areas which contain a lot of edges are selected as characteristic terrain, and then tracking windows are set around the terrain. Though the developed algorithm is advanced and somehow complex, it seems more robust against terrain and illumination condition than FWC, because it uses featured windows, which can be easily tracked.

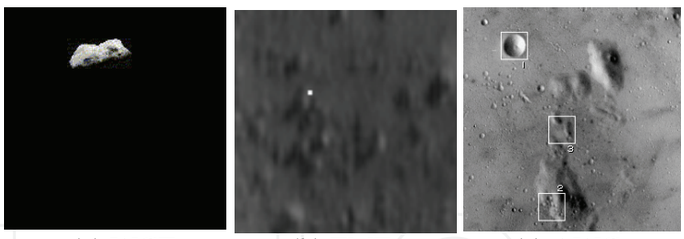

(a) WCT (b) TMT (c) AWC

Figure 13. Image Processing

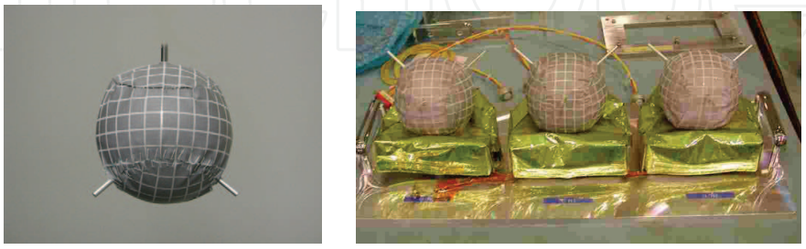

Figure 14. Target Markers

5. Navigation and Control Scheme

5.1 Navigation Scheme

To satisfy the stringent requirement on position and velocity estimation, a navigation filter that utilizes Kalman filter technique (Hashimoto et al., 2001) is adopted. The outputs of the navigation sensors are used to update the propagated states. The update gain is calculated so that the estimation error is minimized. The linearlized state dynamics and observation equations used in the position filter are:

$$x_i=\varphi x_{i-1}+\psi(dv_{i-1}+dv_G),\ \zeta_i=\mathbf{G}(x_{0i})x_i \tag{1}$$

where: (suffix i is omitted)

$$x=(r_{SC/\#}{}^T \quad v_{SC/\#}{}^T)^T \tag{2}$$

$$\varphi=\begin{bmatrix}\mathbf{I}_{3X3} & dT\,\mathbf{I}_{3X3}\\ \mathbf{0}_{3X3} & \mathbf{I}_{3X3}\end{bmatrix}\quad \psi=\begin{bmatrix}(dT/2)\mathbf{I}_{3X3}\\ \mathbf{I}_{3X3}\end{bmatrix} \tag{3}$$

dT :state integration interval
dv_{i-1} :velocity increment measured with ACM
dv_G :estimated gravitational effect

$$\zeta=\zeta^*-g(x_0)+\mathbf{G}(x_0)x_0\ (x_0\text{: current best estimates}) \tag{4}$$

$$\zeta^*=(L\ \ n_X/n_Z\ \ n_Y/n_Z)^T \tag{5}$$

$$\mathbf{G}=\partial \mathbb{g}/\partial \mathbb{x} \tag{6}$$

$$\mathbb{g}(\mathbb{x}) = \begin{pmatrix} \mathbb{r}_{LO/\#} - \mathbb{r}_{SC/\#} \\ (\mathbb{r}_{CO/\#} - \mathbb{r}_{SC/\#})_X/(\mathbb{r}_{CO/\#} - \mathbb{r}_{SC/\#})_Z \\ (\mathbb{r}_{CO/\#} - \mathbb{r}_{SC/\#})_Y/(\mathbb{r}_{CO/\#} - \mathbb{r}_{SC/\#})_Z \end{pmatrix} \tag{7}$$

L : Measurements of LIDAR or LRF
$\mathbb{n}$: Measurement vector of ONCs $=(n_X, n_Y, n_Z)^T$
$\mathbb{r}_{SC}$: Position of the spacecraft
$\mathbb{r}_{LO}$: Position of the range measurement point
$\mathbb{r}_{CO}$: Position of the camera target
$*_{/\#}$: Denotes a vector expressed in navigation reference frame:#
Note) Bold letter such as **φ** denotes a matrix, and $\mathbb{x}$ denotes a vector.
The dynamics and observation equations are processed in Kalman filter algorithm. The propagation of the covariance is executed as follows:

$$\mathbf{P}_i=\varphi\mathbf{P}_{i-1}\varphi^T + \psi\mathbf{Q}_{i-1}\psi^T \tag{8}$$

$$\mathbf{Q}_i = \begin{pmatrix} q_X & 0 & 0 \\ 0 & q_Y & 0 \\ 0 & 0 & q_Z \end{pmatrix} \tag{9}$$

$$q_{X,Y,Z} = kq_V + q_G \tag{10}$$

where:
k : equals 1 when delta V is executed. Otherwise zero
q_V : DeltaV measurement error
q_G : Velocity increment estimation error including gravity and dynamics model error
This filter implementation is applied through all the phases by properly selecting/switching the reference frame and for example, $\mathbb{r}_{CO}$ means the center of the asteroid in high altitude descent phase and TM in final descent phase. $\mathbb{r}_{LO}$ is approximated onboard, by calculating the intersection of laser beam and asteroid shape model.

5.2 Control Scheme

In the final descent and touchdown phase, various operations, such as surface synchronization, attitude alignment to local horizontal surface and stable hovering are required. Six degree-of-freedom variables, three for position and three for attitude, are independently controlled by the thruster control law that utilizes thruster switching curves defined on the phase plane. The outline of the switching curve is shown in Fig.15. In the fine control region, attitude is controlled by RW. Details of the control law have been presented in the paper (Yamashita et al., 2001).

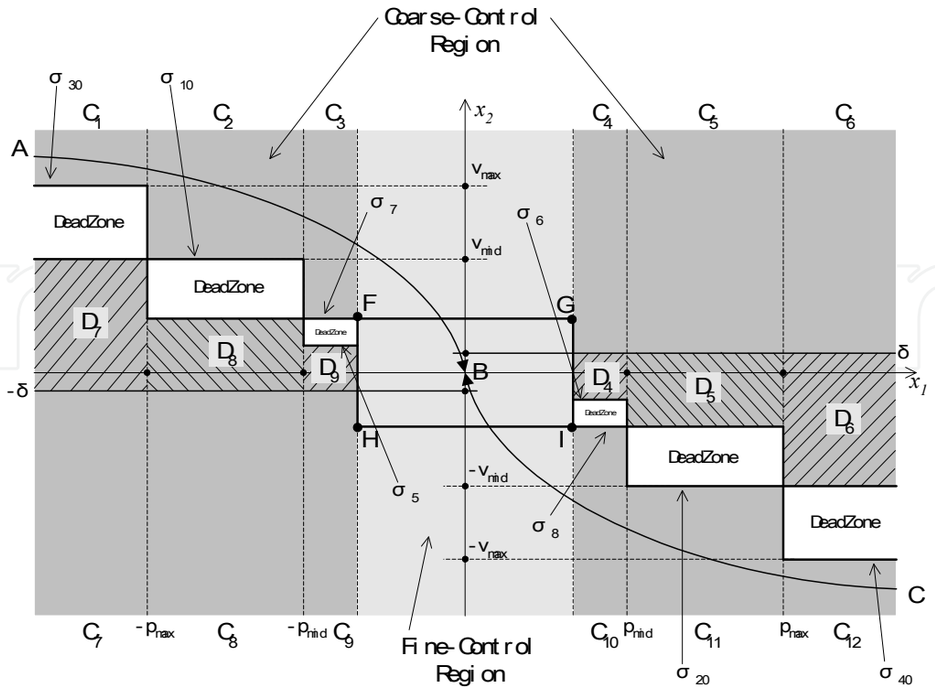

Figure 15. Thruster Switching Curve

6. Flight Results

6.1 Landing Site on Asteroid Itokawa

Figure 16 shows the picture of Itokawa taken by onboard optical navigation camera. The landing and sampling site was selected at the Joint Science Team meeting held in the end of October 2005, considering the scientific interest and the spacecraft safety. From the results on the global mapping of Itokawa from Home Position, it was found that most of the Itokawa surfaces were rocky or steep area, and "Muses-sea" was the only one candidate of landing points are shown by the circle in Fig.16.

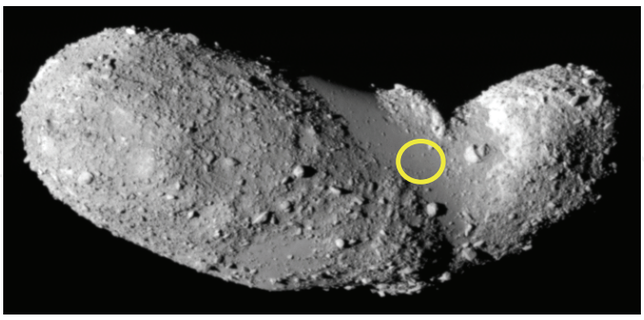

Figure 16. Picture of Itokawa and Landing Site "Muses-sea"

6.2 First Touchdown Results

The first landing for sampling was tried on November 20th 2005. The guidance and the navigation (Kubota et al., 2000) were all performed in order as almost planned. The guidance accuracy was within 30 meters horizontally in terms of the hovering point (Kubota

et al., 2006). The target marker was released at about 40m altitude, because the velocity of target marker was smaller than nominal one and the spacecraft needed more time to get to the surface. The optical navigation camera could track the target marker properly. Figure 17 shows the low-altitude image, in which the shadow of Hayabusa spacecraft on the surface and the shinning released target marker could be seen.
After the obstacle had detected, the spacecraft continued descending because the attitude error was so large enough to prevent ascending the thruster firing. As a result, the spacecraft did unexpected touch-down without sampling sequence, and stayed on the surface for about 34 minutes until the forced ascent was commanded from the ground. The attitude of the spacecraft was controlled during the free-fall and then touchdowns were performed as shown in Fig.18. Therefore natural sample collections seemed to be conducted.

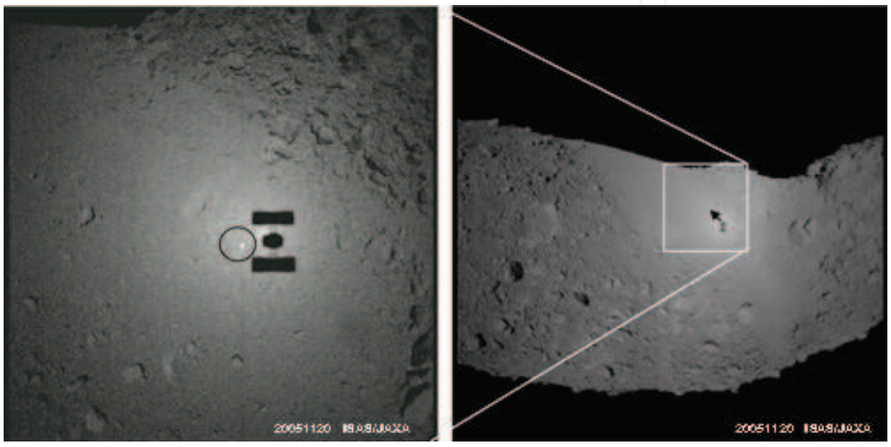

Figure 17. Navigation image taken during descent on 20th Nov. 2005 (Left: taken at 30m altitude, Right: taken at 200m altitude)

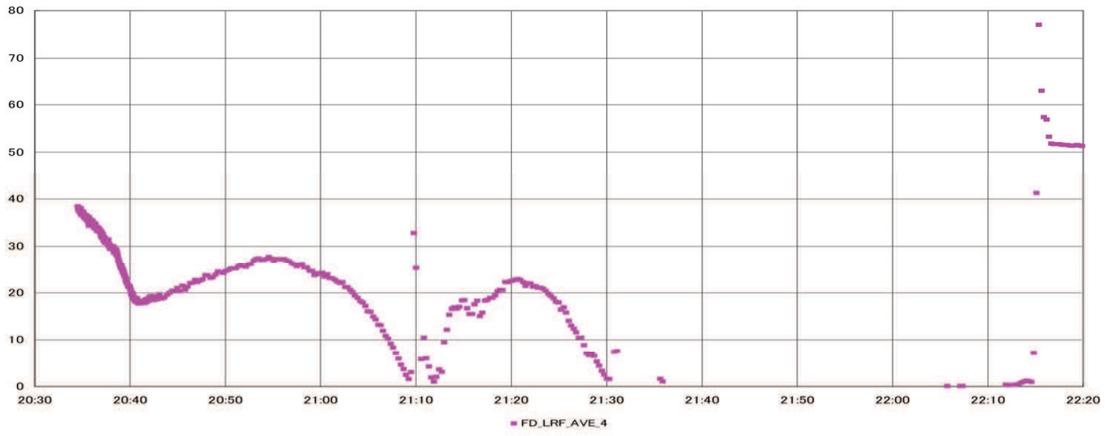

Figure 18. LRF data during bouncing and landing

6.3 Second Touchdown Results

The second and final landing was performed on November 26th 2005 (Yano et al., 2006). The descent path taken was almost same as that at the 1st touching-down attempt, toward the west part of the Muses-sea. As already one TM was in the Muses-sea, to avoid the confusion

for image processing, a new marker was not released, this time. That is, TM was not used for the horizontal speed canceling, because GNC team had confidence to control the spacecraft remotely from the ground station. And also the obstacle detection was not set to be active, but to be monitored, since it seemed reporting too-sensitive signal in the 1st touchdown trial on 20th Nov 2005. The touch-down sequence was set so that the lift off must be only after the sampler horn deformation had detected and the sampling sequence had completed. In the second touchdown trial, the navigation and guidance to the aimed landing point was perfect. Figure 19 shows the image sequence taken by ONC-W1. In Fig.20, TM released on 20th Nov could be seen in the same position. Figure 21 shows the obtained LRF data. Terrain alignment was successfully performed at about 7[m] altitude. Touching-down speed was estimated about 10[cm/second]. When Hayabusa lifted-off, the +Z axis (High Gain Antenna axis) was 7 degrees off from the Sun direction as expected. The communication was established very well and every instrument aboard functioned normally. Though it seemed perfect landing and sampling, after the spacecraft returned to Home Position, it lost the attitude and could not communicate with the high-speed link to the ground stations. Therefore detailed data could not be obtained so far.

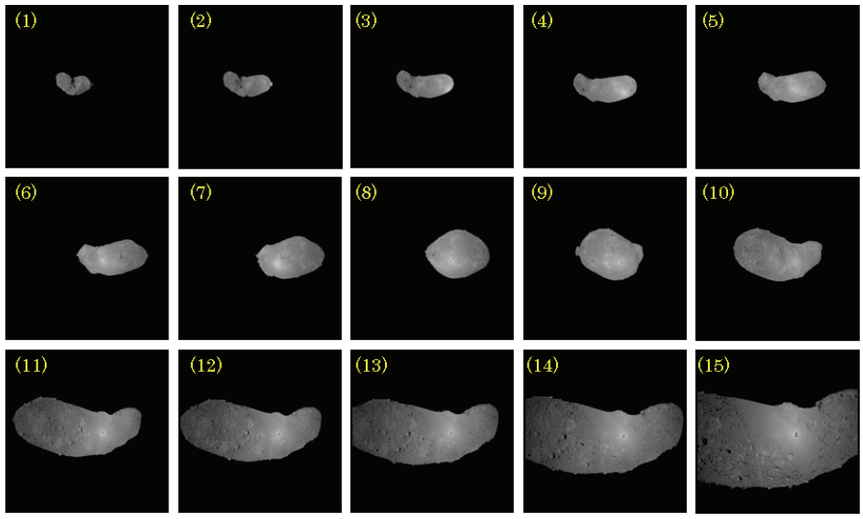

Figure 19. Image Sequence for 2nd Touchdown on 26th Nov. 2005

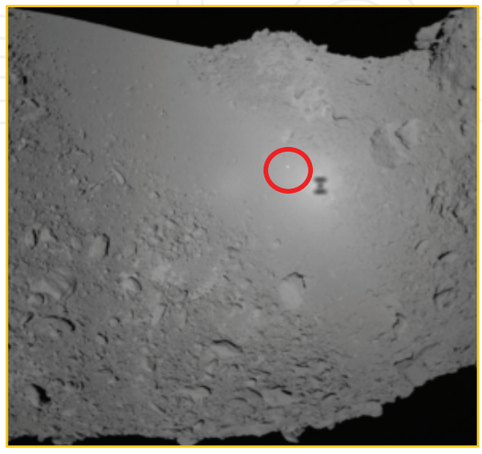

Figure 20. Target Marker released 1st Touchdown in 20th Nov. 2005

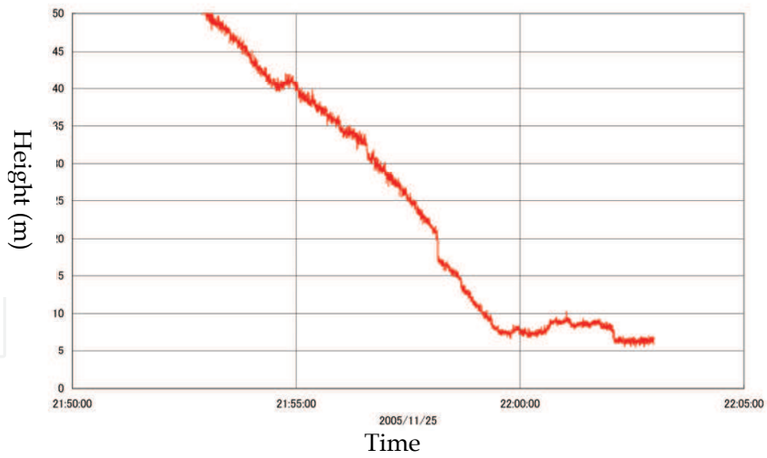

Figure 21. LRF data before touch-down on 26th Nov. 2005

7. Conclusion

This chapter has presented the motion planning of intelligent explorer in Japanese asteroid sample return mission. This chapter explained the navigation sensors and navigation strategy in the descent and touchdown phase for Hayabusa spacecraft. Target marker tracking and attitude alignment have been described in detail. And the flight data showed the effectiveness of the proposed and installed schemes. Hayabusa spacecraft succeeded in touchdown on the surface of Itokawa and lift-off the surface.

8. References

Farquhar, R. (2001). NEAR Shoemaker at Eros : Rendezvous, Orbital Operations, and a Soft Landing. *Advances in the Astronautical Sciences : Astrodynamics 2001*, Vol. 109, 2001, pp. 953-972.

Rayman, M.D. Varghese, P. H.Lehman, D. Livesay, L.L. (2000). Results from the Deep Space 1 Technology Validation Mission. *Acta Astronautica Journal*, vol.47, pp.475-487.

Chiu, M.C. Veverka, J. Reunolds, E.L. (2000). The Contour Mission – Status of Implementation. *IAA Int. Conf. on Low-Cost Planetary Missions*, No.IAA-L-0205.

Atkins, K.L. Martin, B.D. Vellinga, J. Price, R. (2000). STARDUST: Implementing a New Manage-to-Budget Paradigm. *IAA Int. Conf. on Low-Cost Planetary Missions*, No.IAA-L-0202.

Kawaguchi, J. Uesugi, K. Fujiwara, A. (2000). The MUSES-C Mission for the Sample Return - Its Technology Development Status and Readiness. *IAA Int. Conf. on Low-Cost Planetary Missions*, No. IAA-L-0306, 2000.

Wittmann, K. Feuerbacher, B. Ulamec, S. Rosenbauer, H. Bibring, JP. Moura, D. et al., (1999). Rosetta Lander in situ Characterization of a Comet Nucleus. *Acta Astronautica Journal*, Vol. 45, 1999, pp. 389-395.

Kubota, T. Sawai, S. Hashimoto, T. Kawaguchi, J. Fujiwara, A. (2001). Robotics Technology for Asteroid Sample Return Mission MUSES-C. *6th Int. Symposium on Artificial Intelligence, Robotics and Automation in Space*, AS016.

Kawaguchi, J. Uesugi, K. Fujiwara, A. Saitoh, H. (1998). The MUSES-C Mission Description and its Status. *3rd IAA Int. Conf. on Low-Cost Planetary Missions*, IAA-L-98-0505.

Hashimoto, T. Kubota, T. Mizuno, T. (2003). Light Weight Sensors for the Autonomous Asteroid Landing of MUSES-C Mission. *Acta Astronautica*, Vol.52, pp.381-388.

Maruya, M. Ohyama, H. Uo, M. Muranaka, N. Morita, H. Kubota, T. Hashimoto, T. Saito, J. Kawaguchi, J. (2006). Navigation Shape and Surface Topography Model of Itokawa. *AIAA/AAS Astrodynamics Specialist Conference and Exhibit*, 2006-6659.

Hashimoto, T. Kubota, T. Sawai, S. Uo M. (2002). Image-based Guidance, Navigation, and Control for MUSES-C Sample and Return Spacecraft. *Advances in the Astronautical Sciences*, Univelt Inc., Vol. 111, pp. 181-192.

Uo, M. Shirakawa, K. Hashimoto, T. Kubota, T. Kawaguchi, J. (2006). Hayabusa's Touching-down to Itokawa – Autonomous Guidance and Navigation. *AAS2006*, AAS-06-214.

Kubota, T. Sawai, S. Hashimoto, T. Kawaguchi, J. (2007). Collision Dynamics of a Visual Target Marker for Small-body Exploration, *Advanced Robotics*, Vol.21, No.14, pp.1635-1651.

Misu, T. Hashimoto, T. Ninomiya, K. (1999). Optical Guidance for Autonomous Landing of Spacecraft. *IEEE Trans. on Aerospace and Electronic Systems*, Vol.35, No.2, pp.459-473.

Hashimoto, T. Kubota, T. Kawaguchi, J. Uo, M. Baba, K. Yamashita, T. (2001a). Autonomous Descent and Touch-down via Optical Sensors. *Advances in the Astronautical Sciences*, Vol. 108, pp.469-480, Univelt Inc.

Yamashita, T. Uo, M. Hashimoto, T. (2001). Nonlinear Six-degree-of-freedom Control for Flexible Spacecraft. *IFAC Automatic Control in Aerospace*, pp.327-332.

Kubota, T. Hashimoto, T. Sawai, S. Kawaguchi, J. Ninomiya, K. Uo, M. Baba, K. (2000). An Autonomous Navigation and Guidance System for MUSES-C Asteroid Landing. *4th IAA Int. Conf. on Low-Cost Planetary Missions*, IAA-L-307.

Kubota, T. Hashimoto, T. Uo, M. Tsuno, K. Kawaguchi, J. (2006). Use of Laser and Optical Sensors in Terrain Alignment and Touchdowns. *16th AAS/AIAA Space Flight Mechanics Conference*, AAS06-216.

Yano, H. Kubota, T. Miyamoto, H. Okada, T. Scheeres, D. Takagi, Y. Yoshida, K. Abe, M. Abe, S. Barnouin-Jha, O. Fujiwara, A. Hasegawa, S. Hashimoto, T. Ishiguro, M. Kato, M. Kawaguchi, J. Mukai, T. Saito, J. Sasaki, S. Yoshikawa, M. (2006). Touchdown of the Hayabusa Spacecraft at the Muses Sea on Itokawa. *SCIENCE*, Vol.312, pp.1350-1353.

Motion Planning

Edited by Xing-Jian Jing

ISBN 978-953-7619-01-5

Hard cover, 598 pages

Publisher InTech

Published online 01, June, 2008

Published in print edition June, 2008

In this book, new results or developments from different research backgrounds and application fields are put together to provide a wide and useful viewpoint on these headed research problems mentioned above, focused on the motion planning problem of mobile ro-bots. These results cover a large range of the problems that are frequently encountered in the motion planning of mobile robots both in theoretical methods and practical applications including obstacle avoidance methods, navigation and localization techniques, environmental modelling or map building methods, and vision signal processing etc. Different methods such as potential fields, reactive behaviours, neural-fuzzy based methods, motion control methods and so on are studied. Through this book and its references, the reader will definitely be able to get a thorough overview on the current research results for this specific topic in robotics. The book is intended for the readers who are interested and active in the field of robotics and especially for those who want to study and develop their own methods in motion/path planning or control for an intelligent robotic system.

How to reference

In order to correctly reference this scholarly work, feel free to copy and paste the following:

Takashi Kubota, Tatsuaki Hashimoto and Jun'ichiro Kawaguchi (2008). Motion Planning of Intelligent Explorer for Asteroid Exploration Mission, Motion Planning, Xing-Jian Jing (Ed.), ISBN: 978-953-7619-01-5, InTech, Available from: http://www.intechopen.com/books/motion_planning/motion_planning_of_intelligent_explorer_for_asteroid_exploration_mission

INTECH
open science | open minds

InTech Europe
University Campus STeP Ri
Slavka Krautzeka 83/A
51000 Rijeka, Croatia
Phone: +385 (51) 770 447
Fax: +385 (51) 686 166
www.intechopen.com

InTech China
Unit 405, Office Block, Hotel Equatorial Shanghai
No.65, Yan An Road (West), Shanghai, 200040, China
中国上海市延安西路65号上海国际贵都大饭店办公楼405单元
Phone: +86-21-62489820
Fax: +86-21-62489821

IntechOpen